Electromagnetic Analysis of a Synchronous Reluctance Motor with Single Tooth Windings

C M Donaghy-Spargo[1], M*ember, IEEE,* B C Mecrow[2], M*ember, IEEE,* J D Widmer[2], M*ember, IEEE*

[1]Department of Engineering, Durham University, Durham, DH1 3LE, UK
[2]School of Electrical & Electronic Engineering, Newcastle University, Newcastle upon Tyne, NE1 7RU, UK

This paper explores some key electromagnetic design aspects of a synchronous reluctance motor which is equipped with single tooth windings (i.e. fractional slot-concentrated windings). The analyzed machine, a 6 slot 4 pole motor, utilizes a segmented stator core structure for ease of coil winding, pre-assembly and facilitation of high slot fill factors (~60%). The impact on the motors torque producing capability and its power factor of these inter-segment air-gaps between the stator segments is investigated through 2D FEA studies where it is shown that they have a low impact. From previous studies, torque ripple is a known issue with this particular slot-pole combination of synchronous reluctance motor and the use of two different commercially available semi-magnetic slot wedges are investigated as a method to improve torque quality. An analytical analysis of continuous rotor skewing is also investigated as an attempt to reduce the torque ripple. Finally, it is shown through a combination of 2D & 3D FEA studies in conjunction with experimentally derived results on a prototype machine that axial fringing effects cannot be ignored when predicting the *q*-axis reactance in such machines. A comparison of measured orthogonal axis flux linkages/reactance with 3D FEA studies is presented for the first time.

***Index Terms*— AC motor drives, concentrated winding, finite element method, segmented stator, synchronous reluctance machine**

I. Introduction

Synchronous reluctance motors are becoming an increasingly popular area of research for low speed industrial applications [1-4] and in the form of the permanent magnet assisted variant for automotive traction drives [5-7]. Recent work has tended to focus on the traditional distributed winding variant of synchronous reluctance motor [8-11] which has enjoyed some commercial success within this decade. The authors have proposed the adoption of single tooth windings (usually found in switched reluctance motors) or otherwise known as *fractional slot-concentrated windings* [12,13] in synchronous reluctance technology it has been shown that motoring energy conversion efficiency is increased due to the higher achievable coil fill factors and the unique design options available [12]. The adoption has shown to provide high efficiency, but is accompanied by high torque ripple and lower than normal power factors which are barriers to commercial success. Correct electromagnetic design [13] of synchronous reluctance motors with single tooth windings is required such that the torque ripple is minimized and the power factor is maximized – only then will this particular topology compete commercially with the traditional distributed winding synchronous reluctance motor and its predecessor the induction motor. While other authors have touched on this machine topology, following on for the initial work of the authors, a detailed electromagnetic design study is not found in the literature. This paper aims to fill the gap in the literature by presenting detailed analysis of some of the key design options and issues that arise when fractional slot concentrated windings are adopted. The segmented stator arrangement presented in [13] is analyzed in this paper in terms of the effect that inter-segment airgaps have on the torque producing capability and the power factor of the machine. Semi-magnetic slot wedges are explored for mitigation of torque ripple as well as rotor skewing. Finally a comprehensive magnetic characterization of the orthogonal axis magnetic circuit is presented, comparing 2D & 3D FEA results with measured results from a prototyped machine. The analyzed and prototyped machine is a 4-pole synchronous reluctance motor with single tooth windings consisting of 2 coils per phase and a slots/pole/phase of 0.5. In this paper, the machine is termed the cSynRM for "*concentrated* (wound) Synchronous Reluctance Motor".

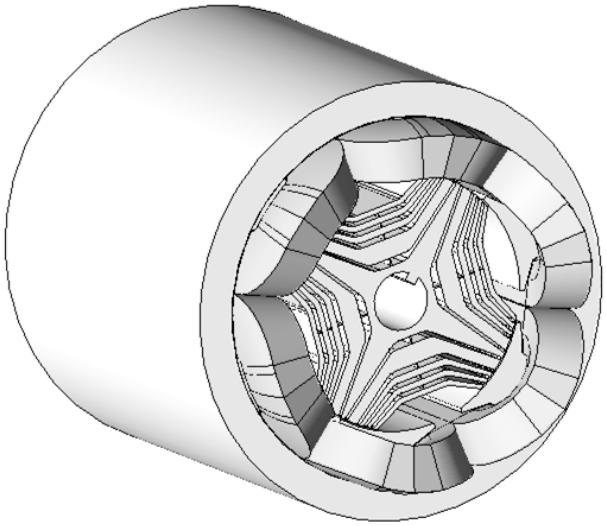

Fig. 1. 3D model of the single tooth wound synchronous reluctance motor

II. Design Specification

This section provides a brief summary of the electromagnetic design of the machine. The outer machine dimensions were chosen to suit the available test-beds, power converters and to be comparable with other machines in-house. The key design parameters are tabulated in Table I. The stator uses a segmented design (Fig. 2); each toothed segment contains a span of stator core, each segment then slots together to form the completed stator core. Inter-segment air-gaps are explored in Section III.

TABLE I
MOTOR DESIGN TABLE

Parameter	Value
Stator outer diameter [mm]	150
Active stack length [mm]	150
Rotor OD [mm]	89
d-axis Mechanical airgap [mm]	0.5
Mechanical Power [kW]	3.6
Base speed [rpm]	1500
DC link voltage [V]	590
Rated current (A)	21.2
Rotor Poles	4
Flux Barriers Per Pole	4
Rib Thickness [mm]	0.3-0.5
Stator Slots	6
Slots/Pole/Phase	0.5
Phase Series Turns	104
Turns per Coil	52
Slot Fill Factor	59%
Fundamental winding factor	0.866

Details of the rotor design can be found in [13] and a detailed comparison of this topology with competing technologies found in [12]. The high slot fill factor is facilitated by concentrated coils and the use of the segmented core back. The winding factors of this slot pole combination are constant at 0.866 and therefore there are significant space harmonics in the airgap field – both odd and even spatial harmonics exist. These harmonic fluxes diminish the power factor due to increased differential leakage inductance and also cause high levels of unwanted torque ripple in the machine. This airgap space harmonic content contributes to the radial B_r and tangential B_θ field components in the airgap;

$$B_{r,\theta}(\theta) = 2\sum_{v=1}^{\infty}\left|B_{rv,\theta v}\right| \Re e\left\{e^{i(v\theta+\widehat{\varphi_v})}\right\} \qquad (1)$$

Here $\widehat{\varphi_v}$ is the phase angle of B_{rv} or $B_{\theta v}$. Then via the Maxwell stress tensor, the torque harmonics can be computed by;

$$T_\theta = \left(\frac{4\pi l_a r^2}{\mu_0}\right)\sum_{v=1}^{\infty}|B_{rv}||B_{\theta v}|\,\Re\mathrm{e}\{e^{i\varphi_{dv}}\} \qquad (2)$$

Here φ_{dv} is the phase angle between B_{rv} & $B_{\theta v}$ and $\pi l_a r^2$ is equal to the rotor electromagnetic volume. Therefore, the key performance criteria of interest in improving such a motor is and impacts upon the power factor and also the torque ripple.

III. INTER-SEGMENT AIRGAP ANALYSIS

In order to obtain the high fill factor, the stator is segmented as in Fig. 2. Segmentation of the stator yoke allows the tooth to be wound before assembly, resulting in fill factors greater than found in distributed winding machines. However, this practice inherently introduces an *inter-segment air gap*, potentially degrading the performance of the machine if not managed (reduced power factor due to the effective airgap lengthening). Assuming these inter-segment gaps are of the same magnitude as the stator core to housing interface gap, which according to [14] has a maximum value of 0.1mm and an average value of 0.037mm, the degradation of the torque and power factor must be assessed. Here, 2D FEA studies are presented for inter-segment interface airgaps between 0 (representing a continuous stator core) and 0.1mm in steps of 0.01mm.

Figure 3 shows the relations between the machine torque and power factor with inter-segment gap length, normalized to zero inter-segment gap length. In the analysis, the stator current fixed at the rated current, rotated at rated speed under maximum torque per ampere current angle. From the figure, it is clear that both the torque and power factor decrease linearly with an increase in inter-segment airgap length. The torque reduces to 94% and the power factor to 97% for the maximum interface gap of 0.1mm corresponding to 20% of the main radial airgap length $\delta = 0.5$mm. In practice it is unlikely that the gap will be large due to the interlocking nature of the core segments and that assembly into the casing (shrink fitted in the case of the prototype) are tightly controlled, the air gaps are expected to be small, if the average value given by [14] is assumed, the machine torque will be at 98% and the power factor at 99% of a machine with a continuous stator core back iron. This suggests that the expected length of inter-segment air gaps have a negligible impact on the performance of the machine. It is concluded that segmented stators are safe to use in machines with small stator-rotor airgaps. In reality, the mechanical tolerance of the segment fit may play a vital role in the length of the inter-segment air gaps.

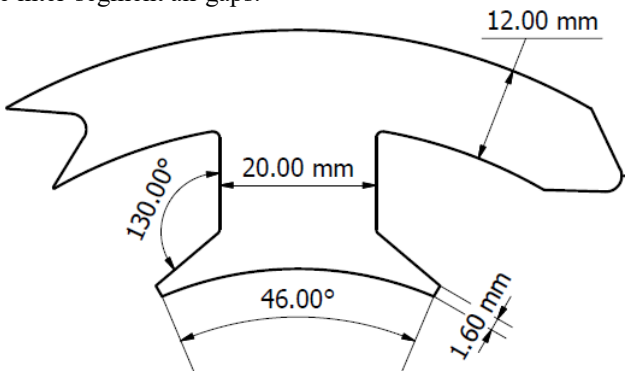

Fig. 2. Stator segment (showing key dimensions and interlocking features)

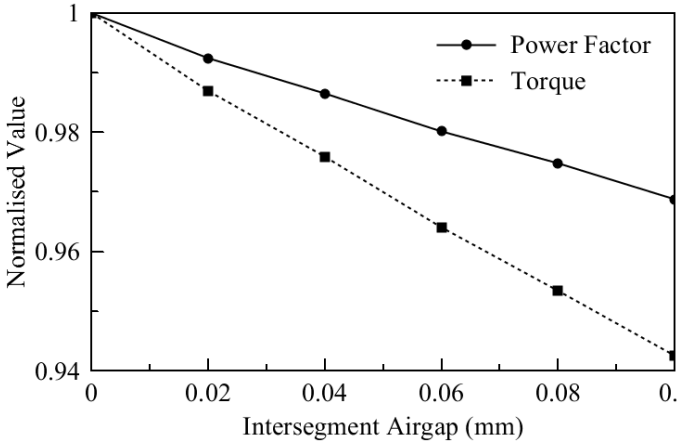

Fig. 3. Torque and power factor variation with inter-segment airgap length

IV. Use of Semi-Magnetic Slot Wedges

Usually, electrical machines use a non-magnetic slot wedge made from either a high temperature plastic or glass fiber that have a relative permeability of $\mu_r = 1$. The primary function of this slot wedge is solely to hold the windings into the stator slot and prevent them from bulging out into the airgap. It has been shown in the literature that switching to a semi-magnetic slot wedge with a low, but >1 relative permeability in the range $2 < \mu_r < 10$ can act to reduce the harmonic content in the airgap by modulating the flux paths – therefore assisting in reducing torque pulsations. Semi-magnetic slot wedges have also used in hydro-generators [15] to improve the EMF harmonic content and in induction machines to improve the losses [16].

In this study, two commercially available semi-magnetic slot wedge materials are compared through 2D FE analysis to ascertain whether such wedges are advantageous in reducing the torque ripple without compromising machine performance. The chosen semi-magnetic wedge materials are commercially available and are known in this paper as *Wedge 1* and *Wedge 2*, their magnetic properties are presented in Figure 4 and their mechanical properties in Table II, taken from the material datasheets supplied by the manufacturers. The 2D finite element study is over a complete electrical cycle at rated current and speed.

TABLE II
Semi-Magnetic Slot Wedge Mechanical Data

Parameter	Wedge 1	Wedge 2
Thickness [mm]	2	2
Compressive Strength [MPa]	160	200
Temperature Class	F (155)	H (180)

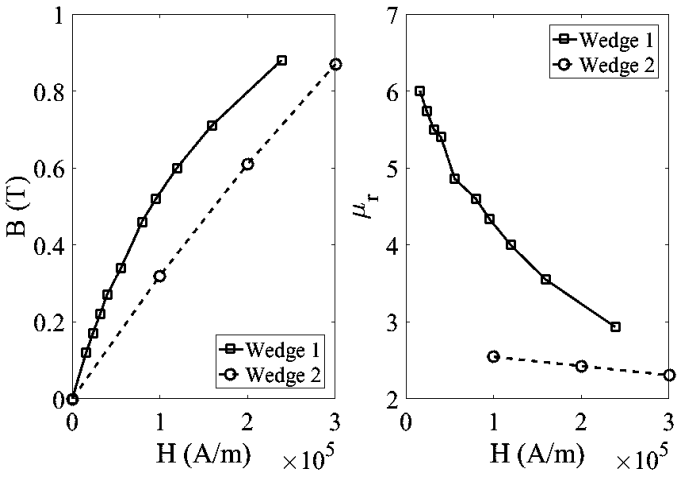

Fig. 4. **B-H** and relative permeability curves of *Wedge 1* & *Wedge 2*

Figure 5 shows the placement of the semi-magnetic slot wedge and Figure 6 shows the results of the FEA studies, considering the relative magnitudes of these performance criteria considered in the study, here δT is the torque ripple. It is clearly evident that the inclusion of the semi-magnetic slot wedge can significantly reduce torque ripple at a little cost of mean torque. However, the tooth tip leakage flux will increase as a result of the semi-permeable bridge across the tooth tips, acting to decrease the power factor of the machine. A simultaneous benefit is the slight reduction of the iron losses, due to the improved harmonic content in the airgap, potentially increasing the efficiency of the machine if wedge loss is minimal (not considered here). The use of wedge *Wedge 1* reduces the mean torque to approximately the same level as the wedge *Wedge 2*, but this second wedge does reduce the torque ripple by the same extent. Quantitatively, by utilizing *Wedge 1* the torque ripple can be reduced by 34.8% to approximately 28% of the mean torque opposed to 44% in a non-magnetic wedged machine, for a mean torque reduction of only 2.6%. In this design, the iron loss in the rotor is reduced significantly by the introduction of semi-magnetic slot wedges, with up to a 20% reduction in rotor iron loss (surface eddy losses) equating to a 3% overall iron loss reduction. The reduction of the torque ripple, and rotor iron losses confirms that the inclusion of the semi-magnetic slot wedges affects mainly the asynchronous harmonic content in the airgap as the mean torque produced by the fundamental flux wave is only slightly affected. However, with these advantages, a reduction in power factor of the machine by up to 4% is observed. The high permeability wedge, *Wedge 1*, has the greatest benefit in terms of torque quality and iron loss reduction, but also delivers the lowest mean torque and lowest power factor, albeit marginally. These results suggest that the inclusion of the semi-magnetic slot wedges is favorable when considering the machine design, effectively reducing the iron loss and the torque ripple.

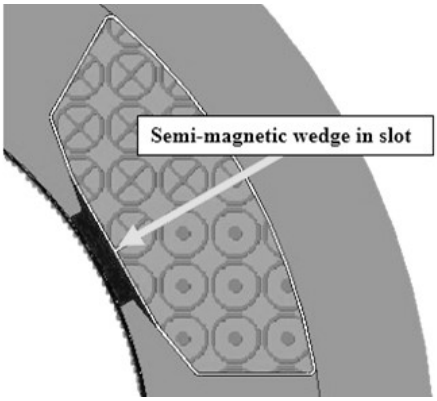

Fig. 5. Semi-magnetic slot wedge placement

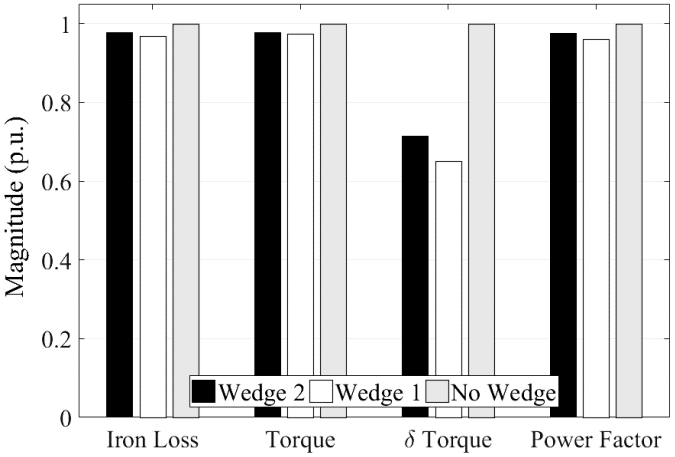

Fig. 6. Torque, power factor and iron loss relative changes when utilizing two different semi-magnetic slot wedges

V. Use of Rotor Skew

Another method of torque ripple reduction is to skew the machines rotor laminations. This acts to average out some of the harmonics to diminish their effect. This technique is usually employed in induction motors but has use in some permanent magnet synchronous machines [17], with 'stepped' skewing becoming popular [7] in automotive traction applications. When skewing, there is an associated harmonic skew factor [18];

$$k_{sqv} = \frac{2\tau_p}{v s\pi} \sin\left(\frac{v s\pi}{2\tau_p}\right) \tag{3}$$

Where s is the skew arc length and τ_p the rotor pole pitch, both in meters; v is the harmonic. Now, in order for the cancellation of the vth harmonic, the following condition must be met;

$$\sin\left(v\frac{s}{\tau_p}\frac{\pi}{2}\right) = 0 \Rightarrow v\frac{s}{\tau_p}\frac{\pi}{2} = k\pi \tag{4}$$

Therefore $k_{sqv} = 0$ and $k \in \mathbb{Z}$. Re-arranging (4) for the skew to effect a vth harmonic cancellation, we set the integer value $k = 1$ and utilize the relationship between the rotor and stator pitches[1] to give the skew as a function of machine parameters. These are the number of stator slots Q_s, the number of rotor pole pairs p, the harmonic v to be cancelled and the stator slot pitch τ_u (or rotor pole pitch τ_p);

$$s = \frac{2\tau_p}{v} = \frac{\tau_u Q_s}{pv} \tag{5}$$

Thus for complete cancellation of the 2nd order harmonic (which is the offending harmonic [13]), the rotor skew arc length must be equal to $1.5\tau_u$ or τ_p meters. Where for $Q_s = 6$, τ_u is equal to 60 mechanical degrees, therefore, $1.5\tau_u$ is equal to 90 mechanical degrees, which is equal to the rotor pole pitch as $2p = 4$. According to Eq. 4 and Figure 7, the second order harmonic falls off slowly and in order to half its contribution, $k_{sq2} = 0.5$, a skew angle of approximately 55 mechanical degrees, $0.9\tau_u$ or $0.6\tau_p$ is required. With this skew, the fundamental component k_{sq1} is approximately equal to 0.85. Therefore, there will be a resulting reduction in mean torque capability due to the modulation of the fundamental skew factor, and ultimately a reduction in the overall fundamental winding factor $k_{w1} = k_{sq1}k_{p1}k_{d1}$, where k_{p1} & k_{d1} are the winding pitch and distribution factors respectively. With no skew, $k_{w1} \approx 0.87$, which is already low [19], and with $k_{sq1} = 0.85$, this is modified to $k'_{w1} \approx 0.73$ which is unacceptably low. If the rotor skew is selected to eliminate the second order harmonic, $k_{sq2} = 0$, the fundamental component $k_{sq1} \approx 0.64$. This reduction in the fundamental outweighs the second order harmonic and thus skew is not warranted in this slot-pole combination for this purpose, it seems that even partial skew is not beneficial due to the choice of slot-pole combination. Due to the negative effects, skew is not analyzed further or implemented in the prototyped motor.

[1] It is easily shown that $\tau_p = (\tau_u Q_s)/(2p)$.

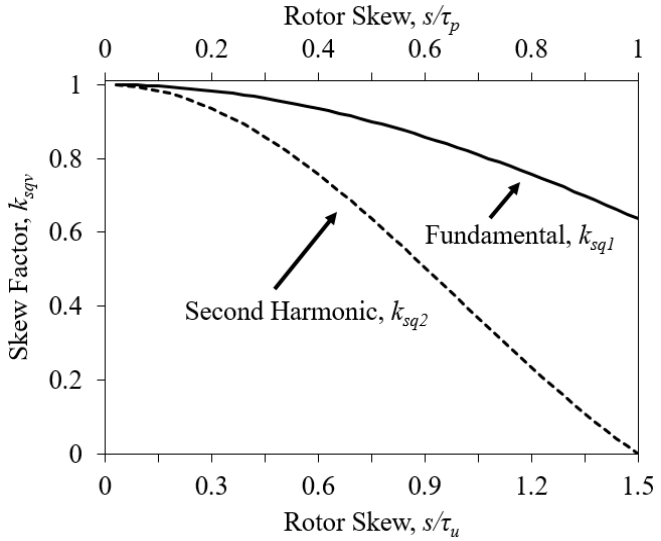

Fig. 7. Skew factors, k_{sq1} & k_{sq2} as functions skew normalized to the rotor pole τ_v and stator slot τ_u pitches

VI. 3D FEA & Experimental Measurements

In previous reports [12,13,19], only 2D FEA studies have been presented. Here, full 3D FEA analysis of the designed machine is presented and compared with experimentally measured results. This section acts to validate the 3D FEA model to be used in subsequent studies. To ensure a fair comparison, the mesh densities in iron components and airgaps within both the 2D and 3D FEA studies were set to be comparable and 2nd order elements were used in both. A high number of refined elements were used in the sliding mesh at the airgap interface. For the experimental results, static locked rotor testing using controlled DC currents was performed on the prototype machine in order to characterize the d- and q-axis flux linkages. The orthogonal axis flux linkages can obtained by integrating the voltage $v[t]$ and current $i[t]$ sample vectors for the d- and q-axis rotor angles θ_d, θ_q and plotting as a function of applied current;

$$\psi_{d,q}[t] = \int_{t=0}^{t} v_{\mathrm{DC}}[t] - i_{\mathrm{DC}}[t]R\, dt \Big|_{\theta=\theta_d,\theta_q} \tag{6}$$

The $i[t]R$ term is used to correct for the winding resistance voltage drop and associated temperature rise due to the injected current pulse-train – numerical integration is used to obtain the flux linkages. Figure 8 shows a comparison of the 2D FEA, 3D FEA and measured d- and q- axis flux linkages. The current range is 2x the rated current. The 2D FEA follows the 3D FEA and experimental direct-axis flux linkages closely due to the simplicity of the flux paths in this rotor position. It is evident that the 2D FEA predicts a lower q-axis flux linkage compared to the 3D FEA and measured results, which show good agreement. This is due to the complexity of the flux paths when magnetizing the q-axis rotor position, leading to more pronounced 3D effects. This effect is similar to that of the magnetization characterization of the switched reluctance

motor in the unaligned position. In this position, due to the complexity of the flux path and air gap in this position the flux tends to 'fringe' in the axial direction. The associated increase in magnetic permeance with this fringing causes an increase in the q-axis inductance and can be modelled as an 'axial fringing factor' f_q describing the increase in permeance due to 3D fringing effects in the q-axis rotor position;

$$L_q = f_q L_{mq} + L_{s\sigma} \tag{7}$$

The L_{mq} term is the magnetizing inductance and the stator leakage inductance is given as $L_{s\sigma}$. The factor f_d also exists, which is the factor describing permeance increase when the rotor is in the d-axis rotor position, though it is negligible due to the small airgap (0.5mm), when compared to the effective airgaps when the rotor is in the q-axis. Obtaining the orthogonal axis flux linkages allows calculation of the orthogonal axis reactances $X_d(i)$ and $X_q(i)$ (see Fig. 9) at the rated operating point $\omega_0 = 2\pi f$, where at rated speed $f = 50$Hz;

$$X_d(i) = \omega_0 \frac{\psi_d(i_d)}{i_d} \quad ; \quad X_q(i) = \omega_0 \frac{\psi_q(i_q)}{i_q} \tag{8}$$

The measured q-axis reactance is higher than the 2D FEA throughout the full current range, matching more closely to the 3D FEA. The error in the 2D FEA is around 10% in the q-axis position. This impacts the power factor and the torque capability of the machine. The instantaneous torque waveform for the rated operating point (current and speed) is presented in Figure 10. The difference in mean torque between the 2D and 3D FEA solutions is 7.1%, giving a 3D FEA mean torque of 20.24Nm compared to the 2D FEA mean torque of 21.73Nm. The lower mean torque is a consequence of the higher q-axis reactance as the torque is computed in the rotating reference frame;

$$T_{em}(i) = \left(\frac{3p}{4\omega_0}\right)\left[X_d(i) - X_q(i)\right] i^2 \sin(\gamma) \tag{9}$$

Where the factor $\left(\frac{3}{4}\right)$ comes from the 3 phase to 2 phase conversion and γ is the current angle. The torque ripple between sees a larger change with the 2D FEA at 39.9% and the 3D FEA torque ripple slightly reduced at 38.7% - the machine did not contain semi-magnetic slot wedges. Dynamic testing of the prototype machine at rated current and speed showed that a mean torque of 19.8Nm was developed at the shaft (this measurement includes rotor windage and bearing friction losses), which agrees closely with the 3D FEA studies – torque ripple was not measured. Any inter-segment airgaps do not appear to have any significant effect and the analysis in Section III is deemed verified through these experimental measurements due to the closeness of the match.

The iron loss components are also calculated in both 2D and 3D FEA studies using a modified Steinmetz Equation and manufacturer's data (See Appendix). The 3D FEA results show a slightly increased iron loss.

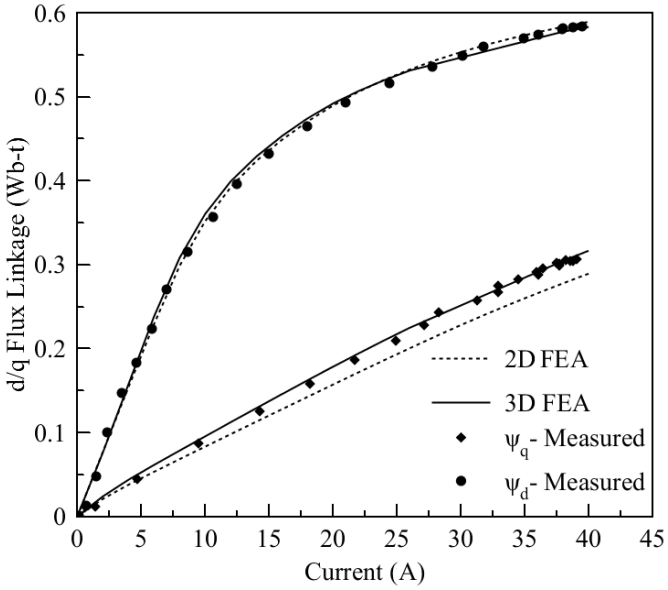

Fig. 8. Orthogonal Axis Flux Linkage Comparison

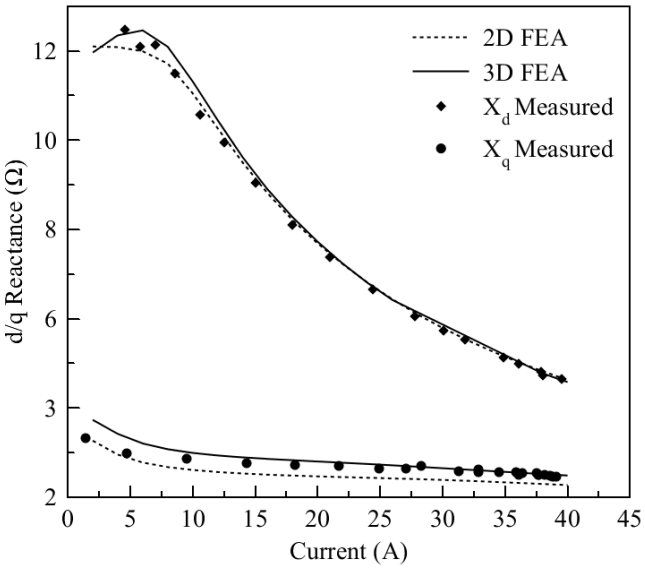

Fig. 9. Orthogonal Axis Reactance Comparison

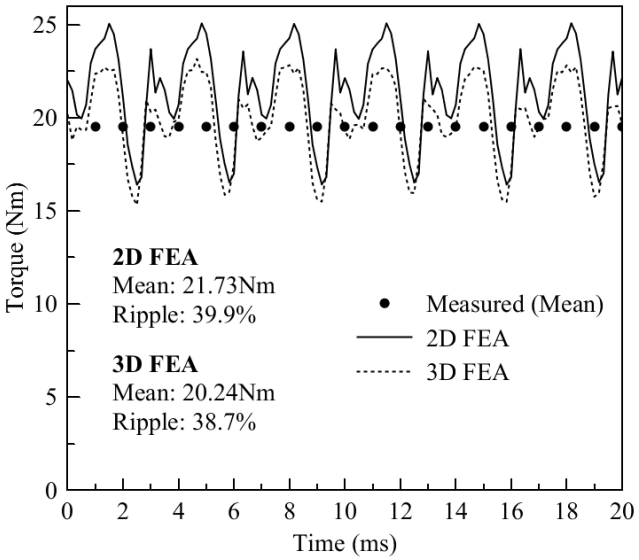

Fig. 10. Instantaneous Torque (Single Electrical Cycle)

Table III presents a separated view of the iron loss between the two FEA solutions. The 3D FEA predicts a 12.8% higher iron loss (eddy current and hysteresis losses) than the 2D FEA model, an increase of total machine loss of only 1.4% as the copper loss is dominant in low speed, low pole number machines. The increase in iron loss can be attributed to the change in magnetic conditions within the machine due to the associated leakage permeance components (end effects) and perhaps the difference in mesh. The 3D modelling shows, however, that while the machine performance is slightly reduced in terms of mean torque increased iron loss, the end effects do not have a large detrimental effect on machine performance.

TABLE III
IRON LOSS COMPARISON

Parameter	2D FEA	3D FEA
Stator Eddy Current [W]	2.85	3.24
Stator Hysteresis [W]	24	26.22
Rotor Eddy Current [W]	2.45	3.02
Rotor Hysteresis [W]	8.37	10.04
Stator Total [W]	26.85	29.46
Rotor Total [W]	10.82	13.06
Motor Total [W]	37.68	42.53

The 3D FEA requires considerable computation time (64 hours) with respect to computation time of the 2D FEA (4 minutes) on a high performance desktop PC (Intel i7 5930K 4.25Ghz, 32GB RAM, the machine is over-clocked and water-cooled). It has 6 physical and 6 additional virtual cores) when the mesh densities are comparable. Second order elements have been used and the field solution is via iterative Newton-Raphson conjugate gradient methods.

VII. PROTOTYPED MOTOR

The motor was prototyped such that magnetic characterization of it would provide data sufficient to validate the numerical modelling. Figure 11 shows the prototyped 4 pole rotor and Figure 12 shows the 6 slot stator in its casing – the flying leads of the double layer single tooth winding can be seen, ready for connection to the terminal ring. The coil end windings are supported by high temperature plastic supports (blue end caps). Each individual coil (52 turns of 2mm diameter copper wire) was wound on each single tooth segment, insulated from the laminations by 0.35mm NOMEX® paper and the six segments were assembled as a whole core before shrink fitting into the aluminum casing. Both the rotor and stator segment laminations were produced using electro-discharge machining techniques, the raw laminations of the stator bonded before cutting the whole stack length of 150mm. This technique is ideal for one-off prototypes but is not suitable due to the slow cutting rate achieved, which was ~1mm/min. The rotor laminations were located on the shaft by the keyway and axially clamped in position with a threaded flange. The most significant challenge in producing the prototype motor was the cutting of the rotor lamination profile due to its numerous fine features, specifically the voids required to be removed to form the flux barriers. It was found that to avoid any difficulties in cutting the laminations, the rotor laminations should be cut by wire electro-discharge machining in axially shorter un-bonded, but clamped, stack lengths (40mm) to facilitate the easy ejection of the removed lamination material -this proved satisfactory. The magnetic characteristics of the prototyped motor matched very closely to that of the finite element studies, see Figures 8-10.

Fig. 11 Rotor of the prototyped machine

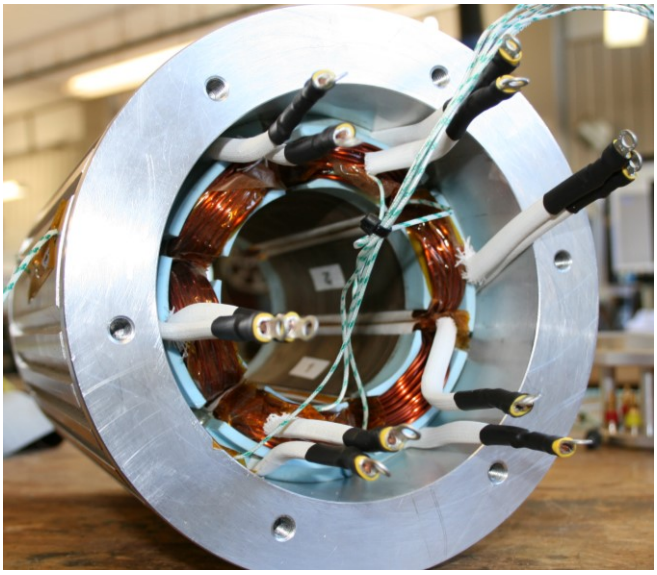

Fig. 12 Stator of the prototyped machine

CONCLUSIONS

This paper has analysed some of the electromagnetic design aspects of a synchronous reluctance motor equipped with single tooth windings. The segmented stator structure and the expected length of inter-segment air-gaps were found to have a negligible effect on the key performance indicators of the machine, the torque density and power factor. It was also shown analytically that skewing the rotor of this particular slot pole combination in order to reduce the toruqe ripple caused by a 2nd order MMF harmonic is not a viable solution due to the severe degradation in the fundamnetal winding factor. A study of semi-magnetic slot wedges showed that respectable improvemnts in torque ripple and iron loss could be achived by using high permeability wedges, with negligible impact on mean torque production and power factor. Finally, a comparison of 2D & 3D FEA studies with experimentally measured results on a prototype machine verified the orthogonal axis inductances. The 2D FEA analysis of this machine was found to be inadequate in predicting the q-axis

inductance due to the significance of the axial fringing – the 3D FEA and experimental results matched closely. With respect to iron loss, while 3D effects appear to play a role in increaseg this loss mechanisim, the machine is low speed and therfore the dominat loss mechanism is the winding copper loss.

APPENDIX

Iron losses were calculated in 2D and 3D FEA using the same method. The local losses (W/kg) in the rotor and stator cores are calculated by the following equation;

$$P_{loss} = \underbrace{k_h f^{\alpha} B^{\beta}}_{\text{Hysteresis}} + \overbrace{k_e (sfB)^2}^{\text{Eddy}}$$

Where f is the electrical frequency, s is a lamination thickness ratio. The material used in the machine model and prototype was M250-35A with the following coefficients and exponents (obtained by curve fitting manufacturer Loss (W/kg) vs. B_{peak} and frequency);

TABLE IV
IRON LOSS CONSTANTS FOR M250-35A

Parameter	Value
Hysteresis Coefficient, k_h	0.0777985
Frequency Exponent, α	1.23089
Field Exponent, β	1.79026
Eddy Coefficient, k_e	3.1454×10^{-5}

ACKNOWLEDGMENT

The authors would like to thank EPSRC for their financial support and also Cummins Generator Technologies, UK for their financial support during this work. The 2D and 3D electromagnetic FEA studies were conducted using Infolytica MagNet and Motorsolve.

REFERENCES

[1] M. H. Mohammadi, T. Rahman, R. Silva, M. Li and D. A. Lowther, "A Computationally Efficient Algorithm for Rotor Design Optimization of Synchronous Reluctance Machines," in *IEEE Transactions on Magnetics*, vol. 52, no. 3, pp. 1-4, March 2016

[2] F. Martin, A. Belahcen, A. Lehikoinen and P. Rasilo, "Homogenization Technique for Axially Laminated Rotors of Synchronous Reluctance Machines," in *IEEE Transactions on Magnetics*, vol. 51, no. 12, pp. 1-6, Dec. 2015

[3] Y. Wang, D. Ionel, D. G. Dorrell and S. Stretz, "Establishing the Power Factor Limitations for Synchronous Reluctance Machines," in *IEEE Transactions on Magnetics*, vol. 51, no. 11, pp. 1-4, Nov. 2015

[4] M. N. Ibrahim, P. Sergeant and E. M. Rashad, "Synchronous Reluctance Motor Performance Based on Different Electrical Steel Grades," in *IEEE Transactions on Magnetics*, vol. 51, no. 11, pp. 1-4, Nov. 2015

[5] H. Huang, Y. S. Hu, Y. Xiao and H. Lyu, "Research of Parameters and Antidemagnetization of Rare-Earth-Less Permanent Magnet-Assisted Synchronous Reluctance Motor," in *IEEE Transactions on Magnetics*, vol. 51, no. 11, pp. 1-4, Nov. 2015

[6] W. Zhao, D. Chen, T. A. Lipo and B. I. Kwon, "Performance Improvement of Ferrite-Assisted Synchronous Reluctance Machines Using Asymmetrical Rotor Configurations," in *IEEE Transactions on Magnetics*, vol. 51, no. 11, pp. 1-4, Nov. 2015

[7] P. Lazari, J. Wang and B. Sen, "3-D Effects of Rotor Step-Skews in Permanent Magnet-Assisted Synchronous Reluctance Machines," in *IEEE Transactions on Magnetics*, vol. 51, no. 11, pp. 1-4, Nov. 2015

[8] Matsuo, T.; Lipo, T.A.; , "Rotor design optimization of synchronous reluctance machine," Energy Conversion, IEEE Transactions on , vol.9, no.2, pp.359-365, Jun 1994

[9] Moghaddam, Reza R.; Magnussen, F.; Sadarangani, C.; , "Novel rotor design optimization of synchronous reluctance machine for high torque density," Power Electronics, Machines and Drives (PEMD 2012), 6th IET International Conference on , vol., no., pp.1-4, 27-29 March 2012

[10] Brown, Geoff; , "Developing synchronous reluctance motors for variable speed operation," Power Electronics, Machines and Drives (PEMD 2012), 6th IET International Conference on , vol., no., pp.1-6, 27-29 March 2012

[11] Kostko, "Polyphase Reaction Synchronous Motor", Journal of AIEE, vol 42, 1923, pp. 1162-1168

[12] C. M. Spargo, B. C. Mecrow, J. D. Widmer and C. Morton, "Application of Fractional-Slot Concentrated Windings to Synchronous Reluctance Motors," in *IEEE Transactions on Industry Applications*, vol. 51, no. 2, pp. 1446-1455, March-April 2015

[13] C. M. Spargo, B. C. Mecrow and J. D. Widmer, "A Seminumerical Finite-Element Postprocessing Torque Ripple Analysis Technique for Synchronous Electric Machines Utilizing the Air-Gap Maxwell Stress Tensor," in *IEEE Transactions on Magnetics*, vol. 50, no. 5, pp. 1-9, May 2014

[14] Staton, Dave, Aldo Boglietti, and Andrea Cavagnino. "Solving the more difficult aspects of electric motor thermal analysis in small and medium size industrial induction motors." *Energy Conversion, IEEE Transactions* on 20, no. 3 (2005): 620-628

[15] L. Yan-ping and Y. Qing-shuang, "Analysis and calculation of electromagnetic force on damper windings for 1000MW hydro-generator," *2011 International Conference on Electrical Machines and Systems*, Beijing, 2011, pp. 1-6.

[16] Anazawa, Y.; Kaga, A.; Akagami, H.; Watabe, S.; Makino, M., "Prevention of harmonic torques in squirrel cage induction motors by means of soft ferrite magnetic wedges," Magnetics, IEEE Transactions on, vol.18, no.6, pp.1550,1552, Nov 1982

[17] X. Ge; Z. Q. Zhu; G. Kemp; D. Moule; C. Williams, "Optimal Step-Skew Methods for Cogging Torque Reduction Accounting for 3-Dimensional Effect of Interior Permanent Magnet Machines," in *IEEE Transactions on Energy Conversion* , vol.PP, no.99, pp.1-1

[18] Pyrhonen, J., T. Jokinen, and V. Hrabovcová. "Design of Rotating Machines." (2008)

[19] C. M. Spargo, B. C. Mecrow, J. D. Widmer, C. Morton and N. J. Baker, "Design and Validation of a Synchronous Reluctance Motor With Single Tooth Windings," in *IEEE Transactions on Energy Conversion*, vol. 30, no. 2, pp. 795-805, June 2015

Christopher M. Donaghy-Spargo received the BEng (Hons) and PhD degrees in Electrical Engineering from Newcastle University, Newcastle upon Tyne, U.K. He was a Motor Drives Engineer (Research) at Dyson, UK, before entering his current position where he is currently an Assistant professor in the field of Electrical Engineering within the Energy Research Group in the Department of Engineering, Durham University, UK. His research interests include the design, modelling and control of high efficiency and high performance electrical machines, with a specific interest in synchronous reluctance machines. He is actively involved with the Institution of Engineering and Technology, UK.

Barrie C. Mecrow received the Ph.D. degree from the University of Newcastle upon Tyne, Newcastle upon Tyne, U.K., for his research into 3-D eddy-current computation applied to turbogenerators. He commenced his career as a Turbogenerator Design Engineer with NEI Parsons, Newcastle upon Tyne, U.K. He became a Lecturer in 1987 and a Professor in 1998 with Newcastle University, Newcastle upon Tyne. He is the Head of the School of Electrical and Electronic Engineering, Newcastle University, where he is also a Professor of electrical power engineering. His research interests include fault-tolerant drives, high-performance permanent-magnet machines, and novel switched reluctance drives.

James D. Widmer is responsible for Newcastle University's 'Centre for Advanced Electrical Drives'. Part of the University's Power Electronics, Drives and Machines Research group, the Centre works with numerous Industry partners to convert academic research into world class products. James' research interests include rare-earth magnet free motor topologies for the automotive industry, including Switched Reluctance and other Motor types, as well as including research into high performance and high efficiency Permanent Magnet machines. James joined Newcastle University in 2009 from a senior post in the Aerospace Industry.